ACS APPLIED MATERIALS & INTERFACES

www.acsami.org

Research Article

Appropriate Molecular Interaction Enabling Perfect Balance Between Induced Crystallinity and Phase Separation for Efficient Photovoltaic Blends

Huanxiang Jiang, Xiaoming Li, Huan Wang, Gongyue Huang, Weichao Chen,* Rui Zhang,* and Renqiang Yang*

Cite This: https://dx.doi.org/10.1021/acsami.0c06326

Read Online

ACCESS | Metrics & More | Article Recommendations | Supporting Information

ABSTRACT: Fluorination is a promising modification method to adjust the photophysical profiles of organic semiconductors. Notably, the fluorine modification on donor or acceptor materials could impact the molecular interaction, which is strongly related to the morphology of bulk heterojunction (BHJ) blends and the resultant device performance. Therefore, it is essential to investigate how the molecular interaction affects the morphology of BHJ films. In this study, a new fluorinated polymer PBDB-PSF is synthesized to investigate the molecular interaction in both nonfluorinated (ITIC) and fluorinated (IT-4F) systems. The results reveal that the F−F interaction in the PBDB-PSF:IT-4F system could effectively induce the crystallization of IT-4F while retaining the ideal phase separation scale, resulting in outstanding charge transport. On the contrary, poor morphology can be observed in the PBDB-PSF:ITIC system because of the unbalanced molecular interaction. As a consequence, the PBDB-PSF:IT-4F device delivers an excellent power conversion efficiency of 13.63%, which greatly exceeds that of the PBDB-PSF:ITIC device (9.84%). These results highlight manipulating the micromorphology with regard to molecular interaction.

KEYWORDS: *molecular interaction, induced crystalline, phase separation, fluorination, synergistic effect*

INTRODUCTION

For solving energy dilemma, polymer solar cells (PSCs) evolved as a prevalent technology because of their unique peculiarity of low toxicity and the potential in fabricating flexible devices.[1−12] Many breakthroughs with power conversion efficiency (PCE) surpassing 17% have been reached with the prosperous evolution of non-fullerene acceptors (NFAs) because of the advantages of their highly tunable optoelectronic properties.[13−24] Notably, elaborately designing photovoltaic materials could profoundly determine the coverage of the solar spectrum and the transport of charge carriers. Introducing the fluorine (F) atom into a donor or an acceptor is deemed as an effectual strategy in fabricating high-performance PSCs as the fluorination could effectively adjust the electronic orbital and optical band gap, which could dissociate the exciton and obtain high open-circuit voltage (V_{OC}).[25−27] Hou designed PM6 by modifying the side chain of PBDTBDD with a fluorine atom. Over 11% PCE was obtained when blended with IDIC.[28,29] Another promising polymer PBTA-PSF was reported with a similar modification method. The resultant photovoltaic device delivered an eminent efficiency approaching 14% owing to the simultaneously achieved high short-circuit current density (J_{SC}) and V_{OC}.[30] Apart from the donor polymer, the fluorination on acceptors has also been proved to be an excellent strategy.[31−33] A fluorinated acceptor IT-4F was synthesized, which yielded an excellent PCE over 13% with PBDB-T-SF.[34] Tang and co-workers reported a fluorine-containing NFA, INPIC-4F, which yields a PCE over 13% in the PBDB-T system.[35] Additionally, the fluorine modification on donor or acceptor materials could impact the molecular interaction, which is strongly related to the morphology of bulk heterojunction (BHJ) blends.[36] For example, Yang and co-workers discovered that the molecular interaction in fluorinated and nonfluorinated systems could result in different miscibilities, which largely influence the charge transport property.[37] Apart from miscibility, the ordered stacking of materials is also decisive in governing charge transport and recombination in PSCs. However, the impact of molecular interaction on the crystalline behavior in fluorinated systems still needs to be explored. Achieving an optimal morphology would be crucial in determining charge

Received: April 6, 2020
Accepted: May 13, 2020
Published: May 13, 2020

transport.[38,39] Moreover, the crystallization process is closely correlated with the phase separation structure in donor/acceptor blend systems. Therefore, exploring the matching principles toward efficient PSCs with regard to molecular interaction crystallinity is significant.

In this contribution, a new copolymer PBDB-PSF based on BDT-PSF[30] was designed and synthesized. Two widely used acceptors, ITIC and IT-4F, were adopted in this study (Figure 1a) to study the impact of molecular interaction on the

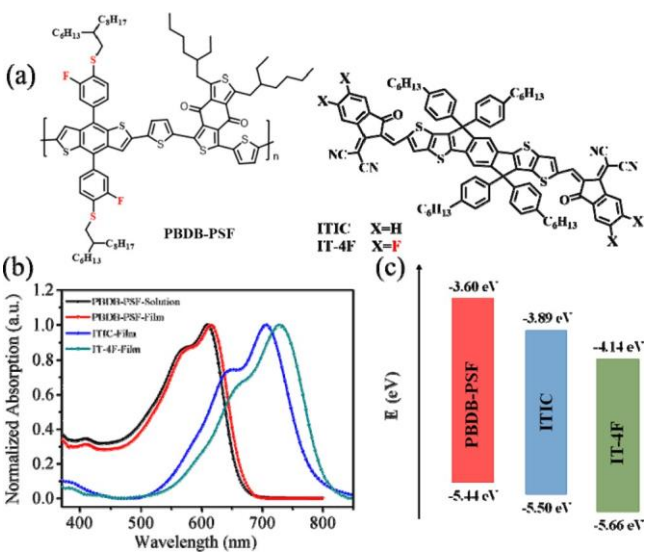

Figure 1. (a) Chemical structures, (b) absorption spectra, and (c) energy-level diagrams of PBDB-PSF, ITIC, and IT-4F.

crystalline property. With the reasonable regulation of molecular interaction, the PBDB-PSF:IT-4F device delivered an excellent PCE (13.63%), which enormously surpassed the PBDB-PSF:ITIC device (9.84%). The superb photovoltaic performance of the IT-4F-based device might be intimately correlated with the morphology: PBDB-PSF:IT-4F exhibits good miscibility with the appropriate phase separation scale, which could be attributed to the balanced interaction between donors and acceptors. More importantly, the F−F interaction between PBDB-PSF and IT-4F may induce the crystallization of IT-4F, thus facilitating the ideal charge transport network. Notably, the crystallization closely correlates with the phase separation and the balance between them could synergistically promote the device performance. Consequently, the IT-4F-based device exhibits excellent charge transport property, thus yielding a high PCE approaching 14%. Our results illustrated that the suitable F−F interaction between the donor and acceptor could synergistically induce the crystallinity of IT-4F and optimize the phase separation scale in the PBDB-PSF:IT-4F system.

RESULTS AND DISCUSSION

The synthetic method of PBDB-PSF is depicted in the Experimental Section. The molecular structures and photophysical properties of PBDB-PSF, ITIC, and IT-4F are illustrated in Figure 1. PBDB-PSF possesses broad absorption (340−690 nm) in both solution and film (E_g^{opt} = 1.83 eV), which complements well with ITIC and IT-4F, thus high J_{SC}'s could be expected in PSCs. A slight red shift was observed in the PBDB-PSF film compared with its solution, reflecting the preaggregation in solution. The highest occupied molecular orbital energy level of PBDB-PSF was about −5.44 eV according to cyclic voltammetry (CV) (Figure S1). The lowest unoccupied molecular orbital (LUMO) energy level was approximately −3.60 eV, suggesting that the driving force in ITIC and IT-4F systems is sufficient for exciton dissociation.

The photovoltaic properties were investigated with the conventional device architecture (Figure 2a, Table 1). A PCE

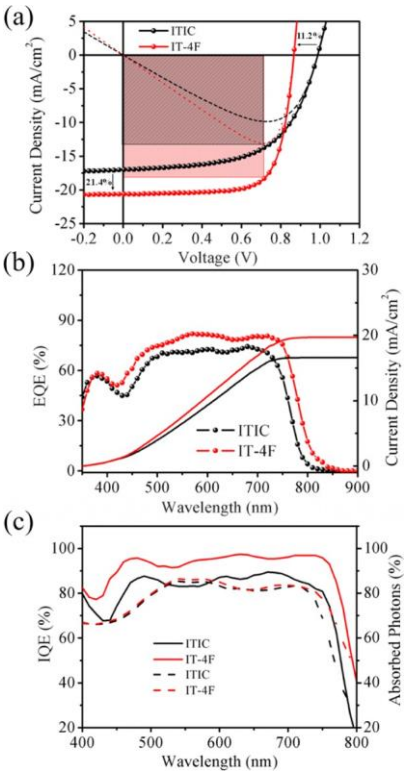

Figure 2. (a) Current density−voltage ($J-V$) curves of optimal PBDB-PSF devices. (b) EQE and the corresponding integrated J_{SC} versus AM 1.5G solar spectrum. (c) Absorption spectra and IQE curves of PBDB-PSF devices (solid lines represent IQE and dashed lines represent absorbed photons).

of 9.84% with a modest J_{SC} (16.99 mA/cm^2) together with an inferior FF (58.73%) was obtained in the PBDB-PSF:ITIC system. Surprisingly, the PBDB-PSF:IT-4F devices yielded an outstanding PCE of 13.63%, with a decent J_{SC} (20.63 mA/cm^2) and a pre-eminent FF (75.10%). It is noteworthy that the IT-4F device showed a slightly decreased V_{OC} for 11.2% value, which may correlate with the lower LUMO of IT-4F. However, J_{SC} exhibited an enormous improvement for about 21.4%. Thus, the maximum power output of the IT-4F-based device reached 13.63 mW/cm^2 along with the remarkably improved FF. The external quantum efficiency (EQE) reflecting photon−electron efficiency in two systems was determined (Figure 2b). The IT-4F-based device exhibited broadened and more intense photoresponse than the ITIC-based device, indicative of more efficient photon conversion and charge transport. Given the EQE and AM 1.5G solar spectrum, the integrated current densities of PBDB-PSF:ITIC and PBDB-PSF:IT-4F devices were about 16.51 and 19.55 mA/cm^2, respectively, matching well with the measured values. The absorption spectra and internal quantum efficiency (IQE) were compared to explore the photocurrent loss. The comparison

https://dx.doi.org/10.1021/acsami.0c06326
ACS Appl. Mater. Interfaces XXXX, XXX, XXX−XXX

Table 1. Device Parameters of Optimal PBDB-PSF-Based Cells[a]

acceptor	V_{OC} [V]	J_{SC} [mA/cm^2]	FF [%]	PCE [%]	μ_e/μ_h [10^{-4} cm V^{-1} s^{-1}]
ITIC	0.99 (0.99 ± 0.01)	16.99 (16.47 ± 0.48)	58.73 (58.23 ± 0.63)	9.84 (9.49 ± 0.43)	0.89/1.64
IT-4F	0.88 (0.88 ± 0.01)	20.63 (20.21 ± 0.58)	75.10 (74.87 ± 0.32)	13.63 (13.35 ± 0.30)	2.75/2.20

[a]The data were obtained from 20 devices.

between IQE and absorption spectra of devices could effectively reflect the degree to which absorbed photons can be converted into photocurrent. The PBDB-PSF:IT-4F device showed a similar absorption intensity with PBDB-PSF:ITIC. However, the IQE of the PBDB-PSF:IT-4F device (~97%) was much higher than that of the PBDB-PSF:ITIC device (~85%), indicative of higher photon conversion efficiency in the IT-4F-based device (Figure 2c).[40,41] As a result, the different photocurrent loss in the two systems may largely account for the different device performance. To further explore the mechanism of current loss, more detailed studies on charge transport and micromorphology were carried out.

Water contact angle (WCA) measurement was carried out to estimate the influence on molecular interaction via fluorination. The WCAs of PBDB-PSF, ITIC, and IT-4F neat films were 105.24, 89.78, and 93.69° (Figure S2), respectively. According to Flory−Huggins theory, the closer the surface energy is, the better the miscibility becomes. Therefore, the PBDB-PSF exhibited stronger interaction with IT-4F than ITIC, which may result in better miscibility in the PBDB-PSF:IT-4F system. These results indicate that the PBDB-PSF:IT-4F film may exhibit good microstructure and hence promote the charge carrier transportation.[42,43]

Photoluminescence (PL) was conducted to probe into the origin of high J_{SC} in the PBDB-PSF:IT-4F device. The PBDB-PSF:IT-4F blend film shows stronger PL quenching than PBDB-PSF:ITIC, indicative of the larger contact surface between the donor and acceptor and higher exciton dissociation efficiency (Figure 3a, excited at 550 nm).[44,45] The J_{SC} with respect to light intensity (I) was studied. They conform to the formula "$J_{SC} \approx I^{\alpha}$", where α indicates the extent of nongeminate charge recombination. α was 0.93 and 0.98 for PBDB-PSF:ITIC and PBDB-PSF:IT-4F systems, respectively. Thus, nongeminate recombination was alleviated in the PBDB-PSF:IT-4F system. The overall charge collection of the devices was characterized by plotting photocurrent density (J_{ph}) at various effective voltages (V_0-V).[8] The J_{ph}'s of both PBDB-PSF:ITIC and PBDB-PSF:IT-4F devices approach to saturation (J_{sat}) at large reverse bias (>2 V), indicating that a large majority of charge carriers were successfully dissociated (Figure 3c). Therefore, the charge extraction probability in PSCs could be characterized by J_{ph}/J_{sat}. Notably, the J_{ph}/J_{sat} of ITIC and IT-4F systems was 90.27 and 93.22%, respectively. Therefore, smooth charge transport can be expected in the PBDB-PSF:IT-4F device, thus accounting for the high J_{SC} and IQE.[46]

The charge carrier mobilities (μ) were obtained to investigate the impact of molecular interaction on charge transport. Notably, the PBDB-PSF:IT-4F device exhibited higher charge carrier mobility. Besides, the μ_e/μ_h of PBDB-PSF:ITIC and PBDB-PSF:IT-4F devices is 0.54 and 1.25, respectively, manifesting that the charge transport was more balanced in the IT-4F-based device. These results could account for the high FF of the IT-4F-based device (Figure S3, Table 1).[47,48]

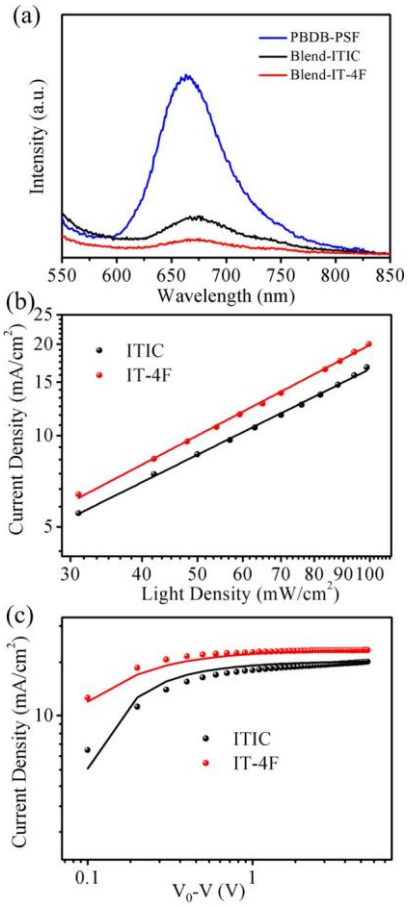

Figure 3. (a) PL of neat PBDB-PSF and blend films. (b) J_{SC} dependence on light intensity. (c) J_{ph} vs V_0-V characteristics (the solid lines are the fitting curves).

The characterization of grazing incidence X-ray diffraction (2D-GIXD) was related to the crystallinity and texture between neat films and blend films.[49,50] Neat films were observed in precedence (Figure S4). The neat PBDB-PSF film exhibited a (100) diffraction peak along the in-plane (IP) direction together with a (010) diffraction peak along the out-of-plane (OOP) direction, which proves that PBDB-PSF adopts face-on orientation. Both (100) and (010) stacking signals appeared in the OOP direction of the neat ITIC film, illustrating the combination of edge-on and face-on orientation. Weak diffraction signals can be observed in the neat IT-4F film, and it is plausible to conclude that IT-4F has the poor crystallinity, given the similar thickness of ITIC and IT-4F films. Some research studies have confirmed that when both the donor and acceptor contain a F atom, a stronger molecular interaction will form.[37] From our results, in the PBDB-PSF:IT-4F blend system, the donor and acceptor had a relatively better compatibility than PBDB-PSF:ITIC, providing more favorable conditions and basis for this F−F interaction. Compared with the GIXD results for neat films mentioned above, the crystalline properties for blend films were probed. As shown

https://dx.doi.org/10.1021/acsami.0c06326
ACS Appl. Mater. Interfaces XXXX, XXX, XXX−XXX

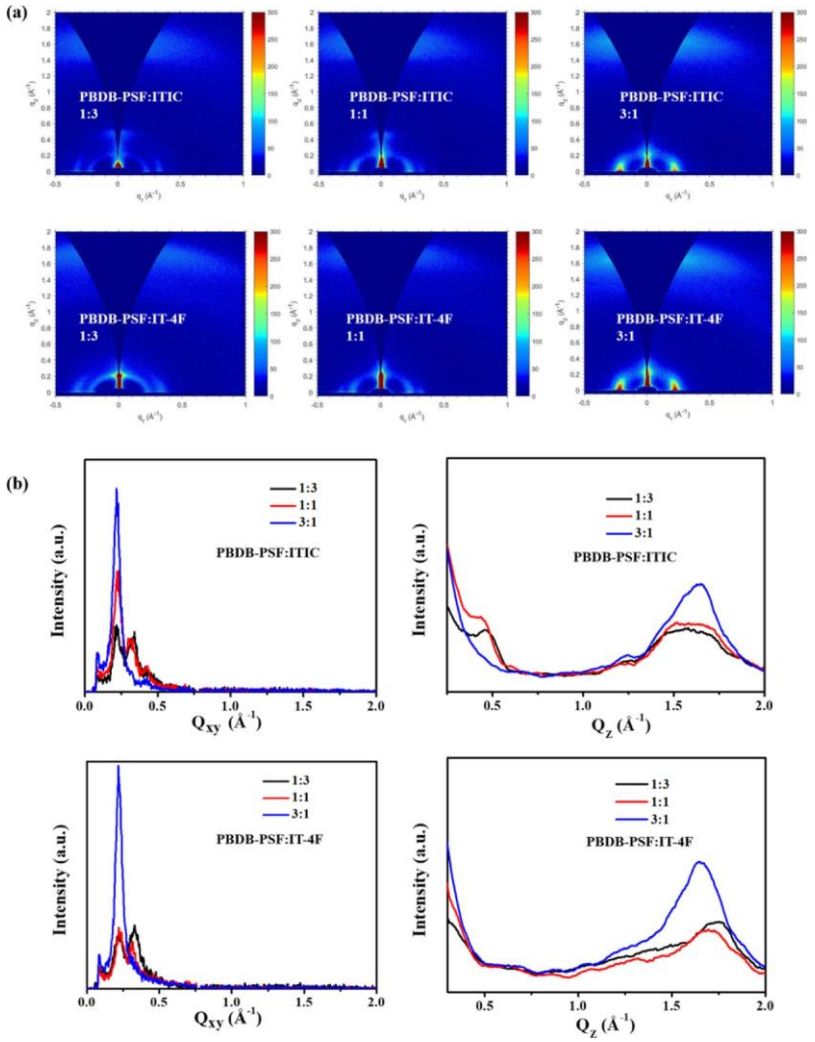

Figure 4. (a) 2D diffraction patterns of blend films with different D/A ratios. (b) Cut line profiles along IP and OOP directions.

in Figure 4, in the PBDB-PSF/IT-4F (1:1 wt %) film, the characteristic peak of PBDB-PSF still appeared at q_{xy} = 0.22 Å^{-1}, but a new diffraction peak appeared at q_{xy} = 0.32 Å^{-1}, which could be attributed to the (100) diffraction peak of IT-4F. However, no obvious change can be observed in the PBDB-PSF:ITIC (1:1 wt %) film, indicating that PBDB-PSF could effectively induce the crystallization of IT-4F. In this manner, the weak crystallinity of IT-4F in the film state is improved. Moreover, the coherence length (CL) of two blend films can be estimated using Scherrer's equation (L_C = 2π/fwhm). The π−π stacking CL in the PBDB-PSF:IT-4F film (28.54 Å) was much larger than that in the PBDB-PSF:ITIC film (15.50 Å) in the OOP direction, presenting better crystallinity, which may be ascribed to the interaction between the donor and acceptor via fluorination. For confirming the existence of this phenomenon, the molecular crystalline behavior in different blend ratio systems was investigated (Figure 4). The similar results were shown, no matter in PBDB-PSF:IT-4F (3:1 wt %) or PBDB-PSF:IT-4F (1:3 wt %) blend systems, which revealed that PBDB-PSF could induce the crystallization of IT-4F, thus being beneficial for achieving a good charge transport network.

Atomic force microscopy (AFM) and transmission electron microscopy (TEM) were employed to characterize the domain size and morphology of active layers. Both films showed an

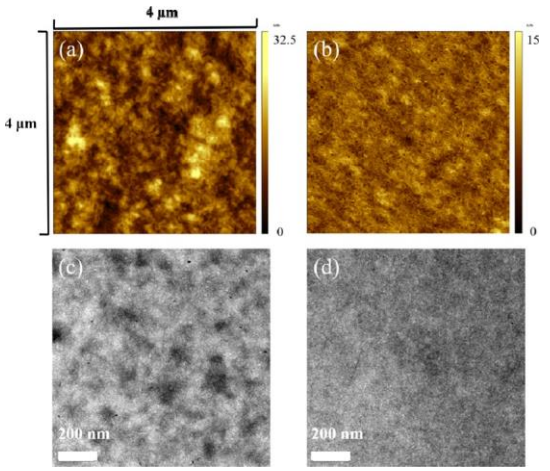

Figure 5. (a) AFM images of PBDB-PSF:ITIC; (b) AFM images of PBDB-PSF:IT-4F; (c) TEM images of PBDB-PSF:ITIC; and (d) TEM images of PBDB-PSF:IT-4F.

obvious fibrous crystal. In addition, the fibrous crystal of the PBDB-PSF:IT-4F blend with a root-mean-square (RMS) = 1.56 nm was more slender than the PBDB-PSF:ITIC blend (RMS = 3.87 nm), which may correlate with the crystallinity of

https://dx.doi.org/10.1021/acsami.0c06326
ACS Appl. Mater. Interfaces XXXX, XXX, XXX−XXX

ITIC and IT-4F. The strong crystalline nature of ITIC might lead to the large aggregation. However, the induced IT-4F crystallization provides the suitable fiber crystal size, which resulted in the appropriate scale of phase separation. These results correspond well with the WCA and PL results. As a consequence, a fluent charge transport network can be expected for IT-4F-based cells, which may be the important factor for the high EQE. Therefore, it is plausible to conclude that despite the poor crystallinity of IT-4F, the F−F interaction could effectively induce the crystallization of IT-4F during the film-forming process and guarantee the equilibrium between miscibility and crystallinity, which is conducive for efficient charge transport.

CONCLUSIONS

In summary, a new polymer PBDB-PSF was synthesized to investigate the molecular interaction in both nonfluorinated (ITIC) and fluorinated (IT-4F) systems and its impact on the crystallinity. Surprisingly, we found that the F−F interaction in the PBDB-PSF:IT-4F system could induce the crystallization of IT-4F and result in the favorable phase separation scale, thus leading to desirable morphology. Consequently, high PCE approaching 14% was achieved in PBDB-PSF:IT-4F devices. Our work emphasizes a distinct perspective in manipulating crystallinity and phase separation with regard to molecular interaction.

EXPERIMENTAL SECTION

Materials and Reagents. The monomer BDT-PSF (compound A) was synthesized formerly in our laboratory. 1,3-Bis(5-bromothiophen-2-yl)-5,7-bis(2-ethylhexyl)-4*H*,8*H*-benzo[1,2-*c*:4,5-*c*′]-dithiophene-4,8-dione (compound B), ITIC, and IT-4F were purchased from Solarmer Materials Inc. Other chemicals were all purchased commercially and used as received.

Synthesis of Polymer PBDB-PSF. Compound A (121.7 mg, 0.1 mmol), compound B (76.7 mg, 0.1 mmol), $Pd_2(dba)_3$ (1.5 mg), and P(*o*-tol)$_3$ (3 mg) were added into a flask. The flask underwent the argon purge for 10 min, next 6 mL of dry toluene was injected into it, and then the solution was swept with argon for 10 min. The reaction mixture was stirred at 110 °C for 2 h. Then, the mixture was cooled to room temperature to precipitate the crude product into methanol. The crude product was filtered and purified by Soxhlet extraction with methanol and *n*-hexane. Finally, the desired polymer was precipitated into methanol from the concentrated CB solution and a purple solid was obtained (Scheme S1, Supporting Information). The number-average molecular weight (M_n) was 28.5 kDa, and the polydispersity index (PDI) was 2.4.

Device Fabrication and Characterization. The preparation of samples, fabrication procedures, and characterization techniques in this work are provided in the Supporting Information.

ASSOCIATED CONTENT

Supporting Information

The Supporting Information is available free of charge at https://pubs.acs.org/doi/10.1021/acsami.0c06326.

Synthetic route of PBDB-PSF; device fabrication procedures; main characterization techniques; TGA, CV, SCLC, and WCA results; and GIXD patterns for neat films (PDF)

AUTHOR INFORMATION

Corresponding Authors

Weichao Chen − *College of Textiles & Clothing, State Key Laboratory of Bio-Fibers and Eco-Textiles, Collaborative Innovation Center for Eco-Textiles of Shandong Province, Qingdao University, Qingdao 266071, China*; Email: chenwc@qdu.edu.cn

Rui Zhang − *Department of Physics, Chemistry and Biology (IFM), Linköping University, Linköping, Sweden*; Email: rui.zhang@liu.se

Renqiang Yang − *Key Laboratory of Optoelectronic Chemical Materials and Devices (Ministry of Education), School of Chemical and Environmental Engineering, Jianghan University, Wuhan 430056, China; CAS Key Laboratory of Bio-based Materials, Qingdao Institute of Bioenergy and Bioprocess Technology, Chinese Academy of Sciences, Qingdao 266101, China*; orcid.org/0000-0001-6794-7416; Email: yangrq@qibebt.ac.cn

Authors

Huanxiang Jiang − *College of Textiles & Clothing, State Key Laboratory of Bio-Fibers and Eco-Textiles, Collaborative Innovation Center for Eco-Textiles of Shandong Province, Qingdao University, Qingdao 266071, China; CAS Key Laboratory of Bio-based Materials, Qingdao Institute of Bioenergy and Bioprocess Technology, Chinese Academy of Sciences, Qingdao 266101, China*

Xiaoming Li − *College of Textiles & Clothing, State Key Laboratory of Bio-Fibers and Eco-Textiles, Collaborative Innovation Center for Eco-Textiles of Shandong Province, Qingdao University, Qingdao 266071, China*

Huan Wang − *College of Textiles & Clothing, State Key Laboratory of Bio-Fibers and Eco-Textiles, Collaborative Innovation Center for Eco-Textiles of Shandong Province, Qingdao University, Qingdao 266071, China*

Gongyue Huang − *Key Laboratory of Optoelectronic Chemical Materials and Devices (Ministry of Education), School of Chemical and Environmental Engineering, Jianghan University, Wuhan 430056, China*

Complete contact information is available at: https://pubs.acs.org/10.1021/acsami.0c06326

Author Contributions

H.J. and X.L. contributed equally to this work. All authors participated in discussion and revision of the final draft.

Funding

The authors deeply appreciate the financial support of the Shandong Provincial Natural Science Foundation, China (ZR2019MF066), the National Natural Science Foundation of China (51773220), and "Chutian Scholar Program" of Hubei province.

Notes

The authors declare no competing financial interest.

REFERENCES

(1) Li, C.; Liu, M.; Pschirer, N. G.; Baumgarten, M.; Müllen, K. Polyphenylene-Based Materials for Organic Photovoltaics. *Chem. Rev.* 2010, *110*, 6817−6855.

(2) Yu, G.; Gao, J.; Hummelen, J. C.; Wudl, F.; Heeger, A. J. Polymer Photovoltaic Cells: Enhanced Efficiencies via a Network of Internal Donor-Acceptor Heterojunctions. *Science* 1995, *270*, 1789−1791.

(3) Huo, L.; Zhang, S.; Guo, X.; Xu, F.; Li, Y.; Hou, J. Replacing Alkoxy Groups with Alkylthienyl Groups: A Feasible Approach to Improve the Properties of Photovoltaic Polymers. *Angew. Chem., Int. Ed.* 2011, *50*, 9697−9702.

(4) Li, G.; Zhu, R.; Yang, Y. Polymer Solar Cells. *Nat. Photonics* 2012, *6*, 153.
(5) Li, X.; Huang, G.; Jiang, H.; Qiao, S.; Kang, X.; Chen, W.; Yang, R. Novel Benzodithiophene Unit with an Alkylthiobiphenyl Side Chain for Constructing High-Efficiency Polymer Solar Cells. *J. Mater. Chem. C* 2019, *7*, 6105−6111.
(6) Li, X.; Liang, Z.; Wang, H.; Qiao, S.; Liu, Z.; Jiang, H.; Chen, W.; Yang, R. Fluorinated D1 (0.5)−A−D2 (0.5)−A Model Terpolymer: Ultrafast Charge Separation Kinetics and Electron Transfer at the Fluorinated D/A Interface for Power Conversion. *J. Mater. Chem. A* 2020, *8*, 1360−1367.
(7) Jiang, H.; Li, X.; Liang, Z.; Huang, G.; Chen, W.; Zheng, N.; Yang, R. Employing Structurally Similar Acceptors as Crystalline Modulators to Construct High Efficiency Ternary Organic Solar Cells. *J. Mater. Chem. A* 2019, *7*, 7760−7765.
(8) Jiang, H.; Li, X.; Wang, J.; Qiao, S.; Zhang, Y.; Zheng, N.; Chen, W.; Li, Y.; Yang, R. Ternary Polymer Solar Cells with High Efficiency of 14.24% by Integrating Two Well-Complementary Nonfullerene Acceptors. *Adv. Funct. Mater.* 2019, *29*, 1903596.
(9) Chen, W.; Shen, W.; Wang, H.; Liu, F.; Duan, L.; Xu, X.; Zhu, D.; Qiu, M.; Wang, E.; Yang, R. Enhanced Efficiency of Polymer Solar Cells by Improving Molecular Aggregation and Broadening the Absorption Spectra. *Dyes Pigm.* 2019, *166*, 42−48.
(10) Jiang, H.; Li, X.; Wang, H.; Ren, Z.; Zheng, N.; Wang, X.; Li, Y.; Chen, W.; Yang, R. Significantly Enhanced Molecular Stacking in Ternary Bulk Heterojunctions Enabled by an Appropriate Side Group on Donor Polymer. *Adv. Sci.* 2020, *7*, 1903455.
(11) An, L.; Tong, J.; Huang, Y.; Liang, Z.; Li, J.; Yang, C.; Wang, X. Elevated Photovoltaic Performance in Medium Bandgap Copolymers Composed of Indacenodi-thieno [3, 2-b] thiophene and Benzothiadiazole Subunits by Modulating the π-Bridge. *Polymers* 2020, *12*, 368.
(12) Li, J.; Liang, Z.; Li, X.; Li, H.; Wang, Y.; Qin, J.; Tong, J.; Yan, l.; Bao, X.; Xia, Y. Insights into Excitonic Dynamic of Terpolymer-Based High-Efficiency Nonfullerene Polymer Solar Cells: Enhance the Yield of Charge Separation States. *ACS Appl. Mater. Interfaces* 2020, *12*, 8475−8484.
(13) Dong, W.-H.; Liu, J.-X.; Mou, X.-J.; Liu, G.-S.; Huang, X.-W.; Yan, X.; Ning, X.; Russell, S. J.; Long, Y.-Z. Performance of Polyvinyl Pyrrolidone-Isatis Root Antibacterial Wound Dressings Produced In Situ by Handheld Electrospinner. *Colloids Surf., B* 2020, *188*, 110766.
(14) Li, J.; Wang, Y.; Liang, Z.; Qin, J.; Ren, M.; Tong, J.; Yang, C.; Yang, C.; Bao, X.; Xia, Y. Non-Toxic Green Food Additive Enables Efficient Polymer Solar Cells Through Adjusting Phase Composition Distribution and Boosting Charge Transport. *J. Mater. Chem. C* 2020, *8*, 2483−2490.
(15) Meng, L.; Zhang, Y.; Wan, X.; Li, C.; Zhang, X.; Wang, Y.; Ke, X.; Xiao, Z.; Ding, L.; Xia, R.; Yip, H.-L.; Cao, Y.; Chen, Y. Organic and Solution-Processed Tandem Solar Cells with 17.3% Efficiency. *Science* 2018, *361*, 1094−1098.
(16) Cui, Y.; Yao, H.; Zhang, J.; Xian, K.; Zhang, T.; Hong, L.; Wang, Y.; Xu, Y.; Ma, K.; An, C.; He, C.; Wei, Z.; Gao, F.; Hou, J. Single-Junction Organic Photovoltaic Cells with Approaching 18% Efficiency. *Adv. Mater.* 2020, *32*, 1908205.
(17) Fan, B.; Zhang, D.; Li, M.; Zhong, W.; Zeng, Z.; Ying, L.; Huang, F.; Cao, Y. Achieving over 16% Efficiency for Single-Junction Organic Solar Cells. *Sci. China: Chem.* 2019, *62*, 746−752.
(18) An, L.; Tong, J.; Yang, C.; Zhao, X.; Wang, X.; Xia, Y. Impact of alkyl side chain on the photostability and optoelectronic properties of indacenodithieno[3,2- b]thiophene- alt -naphtho[1,2- c :5,6- c ′]bis[1,2,5]thiadiazole medium bandgap copolymers. *Polym. Int.* 2020, *69*, 192−205.
(19) Sun, C.; Pan, F.; Chen, S.; Wang, R.; Sun, R.; Shang, Z.; Qiu, B.; Min, J.; Lv, M.; Meng, L.; Zhang, C.; Xiao, M.; Yang, C.; Li, Y. Achieving Fast Charge Separation and Low Nonradiative Recombination Loss by Rational Fluorination for High-Efficiency Polymer Solar Cells. *Adv. Mater.* 2019, *31*, 1905480.
(20) Xu, X.; Feng, K.; Bi, Z.; Ma, W.; Zhang, G.; Peng, Q. Single-Junction Polymer Solar Cells with 16.35% Efficiency Enabled by a Platinum (II) Complexation Strategy. *Adv. Mater.* 2019, *31*, 1901872.
(21) Sun, H.; Liu, T.; Yu, J.; Lau, T.-K.; Zhang, G.; Zhang, Y.; Su, M.; Tang, Y.; Ma, R.; Liu, B. A Monothiophene Unit Incorporating Both Fluoro and Ester Substitution Enabling High-Performance Donor Polymers for Non-Fullerene Solar Cells with 16.4% Efficiency. *Energy Environ. Sci.* 2019, *12*, 3328−3337.
(22) Cui, Y.; Yao, H.; Hong, L.; Zhang, T.; Xu, Y.; Xian, K.; Gao, B.; Qin, J.; Zhang, J.; Wei, Z. Achieving over 15% Efficiency in Organic Photovoltaic Cells via Copolymer Design. *Adv. Mater.* 2019, *31*, 1808356.
(23) Zhan, L.; Li, S.; Lau, T.-K.; Cui, Y.; Lu, X.; Shi, M.; Li, C.-Z.; Li, H.; Hou, J.; Chen, H. Over 17% Efficiency Ternary Organic Solar Cells Enabled by Two Non-Fullerene Acceptors Working in Alloy-Like Model. *Energy Environ. Sci.* 2020, *13*, 635−645.
(24) Ma, R.; Liu, T.; Luo, Z.; Guo, Q.; Xiao, Y.; Chen, Y.; Li, X.; Luo, S.; Lu, X.; Zhang, M. Improving Open-Circuit Voltage by a Chlorinated Polymer Donor Endows Binary Organic Solar Cells Efficiencies over 17%. *Sci. China: Chem.* 2020, *63*, 325−330.
(25) Zhang, Y.; Yao, H.; Zhang, S.; Qin, Y.; Zhang, J.; Yang, L.; Li, W.; Wei, Z.; Gao, F.; Hou, J. Fluorination vs. Chlorination: A Case Study on High Performance Organic Photovoltaic Materials. *Sci. China: Chem.* 2018, *61*, 1328−1337.
(26) Reichenbacher, K.; Süss, H. I.; Hulliger, J. Fluorine in Crystal Engineering"The Little Atom that Could". *Chem. Soc. Rev.* 2005, *34*, 22−30.
(27) Bin, H.; Zhang, Z.-G.; Gao, L.; Chen, S.; Zhong, L.; Xue, L.; Yang, C.; Li, Y. Non-Fullerene Polymer Solar Cells Based on Alkylthio and Fluorine Substituted 2D-Conjugated Polymers Reach 9.5% Efficiency. *J. Am. Chem. Soc.* 2016, *138*, 4657−4664.
(28) Zhang, M.; Guo, X.; Ma, W.; Ade, H.; Hou, J. A Large-Bandgap Conjugated Polymer for Versatile Photovoltaic Applications with High Performance. *Adv. Mater.* 2015, *27*, 4655−4660.
(29) Fan, Q.; Wang, Y.; Zhang, M.; Wu, B.; Guo, X.; Jiang, Y.; Li, W.; Guo, B.; Ye, C.; Su, W. High-Performance As-Cast Nonfullerene Polymer Solar Cells with Thicker Active Layer and Large Area Exceeding 11% Power Conversion Efficiency. *Adv. Mater.* 2018, *30*, 1704546.
(30) Li, X.; Huang, G.; Zheng, N.; Li, Y.; Kang, X.; Qiao, S.; Jiang, H.; Chen, W.; Yang, R. High-Efficiency Polymer Solar Cells Over 13.9% With a High VOC Beyond 1.0 V by Synergistic Effect of Fluorine and Sulfur. *Sol. RRL* 2019, *3*, 1900005.
(31) Dai, S.; Zhao, F.; Zhang, Q.; Lau, T.-K.; Li, T.; Liu, K.; Ling, Q.; Wang, C.; Lu, X.; You, W.; Zhan, X. Fused Nonacyclic Electron Acceptors For Efficient Polymer Solar Cells. *J. Am. Chem. Soc.* 2017, *139*, 1336−1343.
(32) Yao, H.; Cui, Y.; Yu, R.; Gao, B.; Zhang, H.; Hou, J. Design, Synthesis, and Photovoltaic Characterization of a Small Molecular Acceptor with an Ultra-Narrow Band Gap. *Angew. Chem., Int. Ed.* 2017, *56*, 3045−3049.
(33) Jia, B.; Dai, S.; Ke, Z.; Yan, C.; Ma, W.; Zhan, X. Breaking 10% Efficiency in Semitransparent Solar Cells with Fused-Undecacyclic Electron Acceptor. *Chem. Mater.* 2018, *30*, 239−245.
(34) Zhao, W.; Li, S.; Yao, H.; Zhang, S.; Zhang, Y.; Yang, B.; Hou, J. Molecular Optimization Enables Over 13% Efficiency in Organic Solar Cells. *J. Am. Chem. Soc.* 2017, *139*, 7148−7151.
(35) Sun, J.; Ma, X.; Zhang, Z.; Yu, J.; Zhou, J.; Yin, X.; Yang, L.; Geng, R.; Zhu, R.; Zhang, F. Dithieno [3, 2-b: 2′, 3′-d] Pyrrol Fused Nonfullerene Acceptors Enabling over 13% Efficiency for Organic Solar Cells. *Adv. Mater.* 2018, *30*, 1707150.
(36) Ye, L.; Hu, H.; Ghasemi, M.; Wang, T.; Collins, B. A.; Kim, J.-H.; Jiang, K.; Carpenter, J. H.; Li, H.; Li, Z.; McAfee, T.; Zhao, J.; Chen, X.; Lai, J. L. Y.; Ma, T.; Bredas, J.-L.; Yan, H.; Ade, H. Quantitative Relations Between Interaction Parameter, Miscibility and Function in Organic Solar Cells. *Nat. Mater.* 2018, *17*, 253.
(37) Wang, R.; Yuan, J.; Wang, R.; Han, G.; Huang, T.; Huang, W.; Xue, J.; Wang, H. C.; Zhang, C.; Zhu, C.; Cheng, P.; Meng, D.; Yi, Y.; Wei, K. H.; Zou, Y.; Yang, Y. Rational Tuning of Molecular Interaction and Energy Level Alignment Enables High-Performance Organic Photovoltaics. *Adv. Mater.* 2019, *31*, 1904215.

https://dx.doi.org/10.1021/acsami.0c06326
ACS Appl. Mater. Interfaces XXXX, XXX, XXX−XXX

(38) Chen, G.; Sasabe, H.; Igarashi, T.; Hong, Z.; Kido, J. Squaraine Dyes for Organic Photovoltaic Cells. *J. Mater. Chem. A* 2015, *3*, 14517−14534.
(39) Wang, Z.; Yokoyama, D.; Wang, X.-F.; Hong, Z.; Yang, Y.; Kido, J. Highly Efficient Organic P−I−N Photovoltaic Cells Based on Tetraphenyldibenzoperiflanthene and Fullerene C 70. *Energy Environ. Sci.* 2013, *6*, 249−255.
(40) Yuan, J.; Guo, W.; Xia, Y.; Ford, M. J.; Jin, F.; Liu, D.; Zhao, H.; Inganas̈, O.; Bazan, G. C.; Ma, W. Comparing the Device Physics, Dynamics and Morphology of Polymer Solar Cells Employing Conventional PCBM and Non-fullerene Polymer Acceptor N2200. *Nano Energy* 2017, *35*, 251−262.
(41) You, J.; Chen, C. C.; Hong, Z.; Yoshimura, K.; Ohya, K.; Xu, R.; Ye, S.; Gao, J.; Li, G.; Yang, Y. 10.2% Power Conversion Efficiency Polymer Tandem Solar Cells Consisting of Two Identical Sub-Cells. *Adv. Mater.* 2013, *25*, 3973−3978.
(42) Zhang, L.; Xu, X.; Lin, B.; Zhao, H.; Li, T.; Xin, J.; Bi, Z.; Qiu, G.; Guo, S.; Zhou, K.; Zhan, X.; Ma, W. Achieving Balanced Crystallinity of Donor and Acceptor by Combining Blade-Coating and Ternary Strategies in Organic Solar Cells. *Adv. Mater.* 2018, *30*, 1805041.
(43) Lin, Y. L.; Fusella, M. A.; Rand, B. P. The Impact of Local Morphology on Organic Donor/Acceptor Charge Transfer States. *Adv. Energy Mater.* 2018, *8*, 1702816.
(44) Chen, W.; Huang, G.; Li, X.; Wang, H.; Li, Y.; Jiang, H.; Zheng, N.; Yang, R. Side-Chain-Promoted Benzodithiophene-Based Conjugated Polymers Toward Striking Enhancement of Photovoltaic Properties for Polymer Solar Sells. *ACS Appl. Mater. Interfaces* 2018, *10*, 42747−42755.
(45) Chen, W.; Huang, G.; Li, X.; Li, Y.; Wang, H.; Jiang, H.; Zhao, Z.; Yu, D.; Wang, E.; Yang, R. Revealing the Position Effect of an Alkylthio Side Chain in Phenyl-Substituted Benzodithiophene-Based Donor Polymers on the Photovoltaic Performance of Non-fullerene Organic Solar Cells. *ACS Appl. Mater. Interfaces* 2019, *11*, 33173−33178.
(46) Fan, B.; Zeng, Z.; Zhong, W.; Ying, L.; Zhang, D.; Li, M.; Peng, F.; Li, N.; Huang, F.; Cao, Y. Optimizing Microstructure Morphology and Reducing Electronic Losses in 1 cm2 Polymer Solar Cells to Achieve Efficiency over 15%. *ACS Energy Lett.* 2019, *4*, 2466−2472.
(47) Liu, J.; Chen, S.; Qian, D.; Gautam, B.; Yang, G.; Zhao, J.; Bergqvist, J.; Zhang, F.; Ma, W.; Ade, H. Fast Charge Separation In a Non-fullerene Organic Solar Cell With a Small Driving Force. *Nat. Energy* 2016, *1*, 16089.
(48) Wang, H.; Kong, H.; Zheng, J.; Peng, H.; Cao, C.; Qi, Y.; Fang, K.; Chen, W. Systematically Exploring Molecular Aggregation and Its Impact on Surface Tension and Viscosity in High Concentration Solutions. *Molecules* 2020, *25*, 1588.
(49) Müller-Buschbaum, P. The Active Layer Morphology of Organic Solar Cells Probed with Grazing Incidence Scattering Techniques. *Adv. Mater.* 2014, *26*, 7692−7709.
(50) Jiang, Z.; Lee, D. R.; Narayanan, S.; Wang, J.; Sinha, S. K. Waveguide-Enhanced Grazing-Incidence Small-Angle X-Ray Scattering of Buried Nanostructures in Thin Films. *Phys. Rev. B: Condens. Matter Mater. Phys.* 2011, *84*, 075440.

https://dx.doi.org/10.1021/acsami.0c06326
ACS Appl. Mater. Interfaces XXXX, XXX, XXX−XXX